THE FASEB JOURNAL • RESEARCH • www.fasebj.org

Genome-wide effect of pulmonary airway epithelial cell–specific *Bmal1* deletion

Zhenguang Zhang,*[,1] Louise Hunter,* Gang Wu,[†,‡] Robert Maidstone,[§] Yasutaka Mizoro,* Ryan Vonslow,* Mark Fife,[¶] Thomas Hopwood,* Nicola Begley,* Ben Saer,* Ping Wang,[§] Peter Cunningham,* Matthew Baxter,* Hannah Durrington,* John F. Blaikley,* Tracy Hussell,[¶] Magnus Rattray,[§] John B. Hogenesch,[†] Julie Gibbs,* David W. Ray,*[,2,3] and Andrew S. I. Loudon*[,4]

*Centre for Biological Timing, Faculty of Biology, Health, and Medicine, [§]Division of Informatics, Imaging, and Data Sciences, and [¶]Manchester Center for Collaborative Inflammation Research, Faculty of Biology, Health, and Medicine, University of Manchester, Manchester, United Kingdom; and [†]Division of Human Genetics and [‡]Division of Immunobiology, Department of Pediatrics, Center for Chronobiology, Cincinnati Children's Hospital Medical Center, Cincinnati, OH, USA

ABSTRACT: Pulmonary airway epithelial cells (AECs) form a critical interface between host and environment. We investigated the role of the circadian clock using mice bearing targeted deletion of the circadian gene brain and muscle ARNT-like 1 (*Bmal1*) in AECs. Pulmonary neutrophil infiltration, biomechanical function, and responses to influenza infection were all disrupted. A circadian time-series RNA sequencing study of laser-captured AECs revealed widespread disruption in genes of the core circadian clock and output pathways regulating cell metabolism (lipids and xenobiotics), extracellular matrix, and chemokine signaling, but strikingly also the gain of a novel rhythmic transcriptome in *Bmal1*-targeted cells. Many of the rhythmic components were replicated in primary AECs cultured in air-liquid interface, indicating significant cell autonomy for control of pulmonary circadian physiology. Finally, we found that metabolic cues dictate phasing of the pulmonary clock and circadian responses to immunologic challenges. Thus, the local circadian clock in AECs is vital in lung health by coordinating major cell processes such as metabolism and immunity.—Zhang, Z. Hunter, L., Wu, G., Maidstone, R., Mizoro, Y., Vonslow, R., Fife, M., Hopwood, T., Begley, N., Saer, B., Wang, P., Cunningham, P., Baxter, M., Durrington, H., Blaikley, J. F., Hussell, T., Rattray, M., Hogenesch, J. B., Gibbs, J., Ray, D. W., Loudon, A. S. I. Genome-wide effect of pulmonary airway epithelial cell–specific *Bmal1* deletion. FASEB J. 33, 6226–6238 (2019). www.fasebj.org

KEY WORDS: circadian clock · metabolic entrainment · circadian lung function · influenza infection · food entrainment

ABBREVIATIONS: AEC, airway epithelial cell; ALI, air-liquid interface; BAL, bronchoalveolar lavage; BMAL1, brain and muscle ARNT-like 1; CCSP, club cell secretory protein; CLOCK, Circadian Locomotor Output Cycles Kaput; CRY, cryptochrome; CT, circadian time; DE, differentially expressed; KEGG, Kyoto Encyclopedia of Genes and Genomes; LCM, laser-capture microdissection; mTEC, membrane-thermotolerant *Escherichia coli*; PER, period; pfu, plaque-forming unit; qPCR, quantitative PCR; RNA-seq, RNA sequencing; RRE, ROR element; WT, wild type; ZT, zeitgeber time

[1] Current affiliation: Department of Oncology, MRC Research Centre, University of Cambridge, Cambridge, United Kingdom.
[2] Current affiliation: Radcliffe Department of Medicine, University of Oxford, Oxford, United Kingdom.
[3] Correspondence: Centre for Biological Timing, Faculty of Biology, Health and Medicine, University of Manchester, Manchester M13 9PT, United Kingdom. E-mail: david.w.ray@manchester.ac.uk
[4] Correspondence: Centre for Biological Timing, Faculty of Biology, Health and Medicine, University of Manchester, Oxford Rd., Manchester M13 9PT, United Kingdom. E-mail: andrew.loudon@manchester.ac.uk

This is an Open Access article distributed under the terms of the Creative Commons Attribution 4.0 International (CC BY 4.0) (http://creativecommons.org/licenses/by/4.0/) which permits unrestricted use, distribution, and reproduction in any medium, provided the original work is properly cited.

doi: 10.1096/fj.201801682R
This article includes supplemental data. Please visit *http://www.fasebj.org* to obtain this information.

Circadian timekeeping in mammals is regulated by a transcription and translation feedback loop driven by a set of clock proteins. The basic HLH (helix–loop–helix)–PER–ARNT–SIM (bHLH–PAS) domain containing transcriptional activators Circadian Locomotor Output Cycles Kaput (CLOCK) and brain and muscle ARNT-like 1 (BMAL1; also known as ARNTL) drives the expression of hundreds of E-box–driven genes, including the period (PER) and cryptochrome (CRY) genes. The PER and CRY proteins form a complex in the cytoplasm and translocate to the nucleus, where they interact with CLOCK-BMAL1 heterodimers to repress transcription at many loci, including their own. Later, PER and CRY repressors are actively degraded by regulated proteolysis and the cycle starts again. There are 2 ancillary loops that function to fine-tune the clock and shield it from perturbation (1). Uniquely, loss of *Bmal1* leads to complete loss of circadian rhythmicity in behavior and physiology; for this reason, *Bmal1*-null mice are widely used in circadian investigations. However, global knockout of *Bmal1* has severe consequences, including arthropathy, infertility, disrupted metabolic homeostasis, and a reduction in lifespan (2, 3).

0892-6638/19/0033-6226 © The Author(s)
www.fasebj.org by Oxford Univ Lib Serv - Bodleian Lib (163.1.203.50) on June 11, 2019. The FASEB Journal Vol. ${article.issue.getVolume()}, No. ${article.issue.getIssueNumber()}

For this reason, BMAL1 knockout models have limited utility in defining the impact on specific cell types and organs. To address this, many studies have used Cre-LoxP technology to achieve tissue-specific disruption of *Bmal1*, commonly leading to disrupted homeostatic physiology specific to that tissue (4).

There is mounting evidence for an important role of the circadian clock in pulmonary physiology and disease. Repeated phase shifting of environmental lighting schedules (*i.e.*, jet lag or shift work protocols), which is known to disrupt circadian activity and organ-wide rhythmicity, leads to augmented lung tumor formation in p53 knockout mice (5), with a similar phenotype observed in a background of the *Per2* knockout strain. We have previously shown that pulmonary responses to injury such as bleomycin-mediated oxidative damage are augmented in the circadian clock mutant ClockΔ19 mice, driven by dysregulation of the E-box–regulated nuclear factor erythroid-derived 2-like 2 and glutathione-mediated antioxidant defense pathway (6). Global loss of *Bmal1* also leads to hyperinflammatory pulmonary responses to respiratory viral infections (7–9). Selective gene targeting of *Bmal1* within bronchial airway epithelial cells (AECs) causes increased inflammatory responses to smoking (10), whereas our earlier studies have shown impaired pulmonary glucocorticoid signaling, leading to a selective augmentation of specific chemokines and a hyperinflammatory response to LPS (11). Thus, multiple pulmonary pathologies are linked to the circadian clock.

Here, we report the impact of circadian gene targeting using Cre-lox to delete *Bmal1* in club cell secretory protein (CCSP)-expressing pulmonary AECs and reveal widespread perturbation of rhythmic transcriptional control within these cells. *In vivo*, we observed increased background pulmonary neutrophilia and impaired lung biomechanical function. We also observed impaired recovery to pulmonary influenza viral infection with activation of multiple cytokine and chemokine genes.

We next characterized the circadian transcriptome of AECs using laser-capture microdissection (LCM) from *Bmal1*$^{flox/flox}$ and *CCSP-Bmal1*$^{-/-}$ mice over 2 circadian cycles. Rhythmic genes in AECs were enriched for metabolism, cell matrix interaction, and chemokine signaling, the majority of which were disrupted upon *Bmal1* deletion. Strikingly, we also detected an emergent novel rhythmic transcriptome in *Bmal1*-targeted AECs, which lacked enrichment for canonical clock gene–regulating elements, implying that the intact clockwork in these cells may block the imposition of exogenous circadian signals to AECs. Using time-feeding schedules, we show that the pulmonary clockwork and responses to endotoxin challenge are phase reversed when mice are fed in the light phase, indicating a critical role for systemic metabolic cues in entrainment of the pulmonary clock. Finally, we cultured AECs using an air-liquid interface (ALI) culture model, and this revealed a remarkably similar transcriptional mechanism to those of intact tissue, suggesting an important autonomous role for the AEC in pulmonary physiology. Thus, the autonomous circadian clockwork in AECs is indispensable for normal pulmonary homeostasis and innate immunity and is entrained by systemic rhythmic feeding-associated metabolic cues.

MATERIALS AND METHODS

Animals

All experiments on animals were carried out in accordance with the UK Home Office Animals (Scientific Procedures) Act of 1986 and European Directive 2010/63/EU. Mice were group housed under the following controlled conditions: 12-h light/dark cycle at 21°C with free access to standard rodent chow and water unless otherwise stated. *CCSP-Bmal1*$^{-/-}$ and control *Bmal1*$^{flox/flox}$ mice were bred in a *Per2-luc* background. Global *Bmal1*$^{-/-}$ mice were bred by intercrossing of *Bmal1*$^{+/-}$ mice, a gift from Prof. Akhilesh Reddy (University of Cambridge, Cambridge, United Kingdom). C57BL/6 mice were commercially sourced from Envigo (Huntingdon, United Kingdom). All experiments used male mice aged between 10 and 20 wk unless otherwise stated. For collection of tissues in the light/dark cycle, mice were sampled at zeitgeber time (ZT)0–24, which by convention indicates lights on at ZT0. For circadian collections, mice were maintained in constant darkness and samples collected 1 cycle after transfer to darkness at circadian time (CT), which by convention anchors expected time of lights off and activity onset to CT12.

Bronchoalveolar lavage leukocyte count and fluorescence-activated cell-sorting analysis

Bronchoalveolar lavage (BAL) was undertaken as described in Gibbs *et al.* (11). PBS (1 ml) with EDTA (10 mM) was used to lavage the lung *via* a tracheal cannula. Cell concentrations were counted in a NucleoCounter NC-250 machine (Chemometec, Allerod, Denmark) according to the enclosed protocol by mixing 20 μl of the BAL solution with 1 μl solution 18, which were loaded in an A8 slide. The remaining BAL solution was centrifuged at 4°C at 500 *g* for 5 min. After the supernatants were frozen down at −80°C, cells were blocked with anti-CD16/32 antibody (1:100, clone 93, 14-0161-86; Thermo Fisher Scientific, Waltham, MA, USA) and stained with the following antibodies: anti-CD45 pacific blue (1:100, clone 30-F11, MCD4528; Thermo Fisher Scientific), anti-CD11c allophycocyanin (1:200, clone N418, 17-0114-82; Thermo Fisher Scientific) and anti-Ly6g Alexa Fluor 488 (1:200, clone RB6-8C5, 53-5931-82; Thermo Fisher Scientific). Macrophages were gated as $CD45^+$ $CD11c^+$ $Ly6g^-$ cells and neutrophils as $CD45^+$ $CD11c^-$ $Ly6g^+$ cells.

Lung function test

CCSP-Bmal1$^{-/-}$ and control *Bmal1*$^{flox/flox}$ mice (males, n = 3–15, 4 or 12 mo old) were used for lung function tests in flexiVent Fx1 (Scireq, Montreal, Canada). Anesthetic reagents were hypnorm (0.315 mg/ml fentanyl; 10 mg/ml fluanisone) and midazolam (5 mg/ml). They were mixed with water for injection, with a ratio of 1:2:1 (hypnorm, water, and midazolam, respectively), and 0.1 ml/10 g mouse weight was used for intraperitoneal injection. After tracheal cannulation, mice underwent mechanical ventilation with default settings of the machine. The lungs were expanded with deep ventilation, and the pressure volume graph was examined for air flow leakage or voluntary respiration. Then, lung function was measured by the default mechanical scanning protocol and the average value of 3 repeated readings was calculated for comparisons.

www.fasebj.org by Oxford Univ Lib Serv - Bodleian Lib (163.1.203.50) on June 11, 2019. The FASEB Journal Vol. ${article.issue.getVolume()}, No. ${article.issue.getIssueNumber()}

Influenza infection

CCSP-Bmal1$^{-/-}$ and control *Bmal1*$^{flox/flox}$ mice (males, n = 6–10, 10–20-wk-old) were intranasally infected with 5 plaque-forming units (pfu) of influenza A virus, Puerto Rico/8/34, and H1N1 in 50 μl PBS in the morning. Weight was checked every day to monitor disease development. In the first cohort, mice were culled at d 21 postinfection. In a second cohort, mice were culled at d 11 postinfection without BAL sample collection. Left lungs were fixed with 4% paraformaldehyde for paraffin embedding. Right lungs were frozen for RNA. Hematoxylin and eosin staining was performed in lung sections cut at 5-μm thickness, with images obtained from CaseView software (3DHistech, Budapest, Hungary) after scanning slides in Pannoramic 250 Flash III (3DHistech). Lung injury histology scoring was undertaken as previously described in Bayes *et al.* (12), with peribronchial infiltrate from 0 to 4 and alveolar involvement from 0 to 3. Six samples from each group were randomly selected and three ×10 images were scored per mouse.

LCM and RNA sequencing analysis

CCSP-Bmal1$^{-/-}$ and control *Bmal1*$^{flox/flox}$ mice were entrained for 7 d in light/dark cycles (lights on at 7 AM, and lights off at 7 PM) before being kept in constant darkness for 24 h. Lungs were collected every 4 h for 48 h in constant dark conditions with 1 mouse and genotype per time point. LCM of club cells was undertaken as previously described in Betsuyaku *et al.*, with modifications (13). After culling (pentobarbital, intraperitoneally), lungs were inflated with ~0.8 ml 50% optimal cutting temperature/PBS v/v solution *via* a tracheal cannula. Dissected lung samples were frozen on dry ice and stored at −80°C. Samples were cut into 10-μm sections in a cryostat machine onto polyethylene naphthalate membrane slides (11600288; Leica Microsystems, Buffalo Grove, IL, USA). After serial dehydration in ethanol solutions (100, 75, 50, 95, 100, and 100%, 30 s each), slides were air-dried and then dissected in LMD6500 (Leica Microsystems). Distal bronchiolar epithelium was collected ~200 nm from the alveolar opening. RNA was purified by the PicoPure RNA Isolation Kit (Thermo Fisher Scientific) with on-column DNase digestion. RNA integrity was checked by the Agilent RNA 6000 Pico Kit (Agilent Technologies, Santa Clara, CA, USA). Poly (A)-selected mRNA (100 ng total RNA/sample, RNA integrity number ≥6) was used for RNA sequencing (RNA-seq). The library was constructed with TruSeq SBS Kit v.3 (Illumina, San Diego, CA, USA) with low-input method. Samples were sequenced in HiSeq 2500 (Illumina) with 4 samples per lane, generating 100 × 100 base-pair end reads. After filtering and mapping, differentially expressed (DE) genes across all 12 time points were called using DE-Seq2 (14) with a false discovery rate of 0.05. For rhythmic gene detection, MetaCycle (*https://cran.r-project.org/web/packages/MetaCycle/index.html*) (15) was used with meta2d ($P < 0.01$). Kyoto Encyclopedia of Genes and Genomes (KEGG) pathway enrichment analysis was performed by the Database for Annotation, Visualization and Integrated Discovery (DAVID) v.6.8 (*https://david.ncifcrf.gov/*) (16, 17), and gene ontology term analysis was carried out in Enrichr (*https://cran.r-project.org/web/packages/enrichR/index.html*) (18, 19). Phase set enrichment analysis (20) was used to analyze rhythmic pathways at different times of day [$q < 0.05$ with rhythmic genes ($P < 0.05$ by MetaCycle)]. RNA-seq data were stored in Array Express (E-MTAB-6384; European Bioinformatics Institute, Cambridge, United Kingdom; *https://www.ebi.ac.uk/arrayexpress/*). Normalized read counts, rhythmic gene detection, and DE genes are shown in the Supplemental Data.

Western blotting

Mouse lungs were homogenized in RIPA buffer (R0278; MilliporeSigma, Burlington, MA, USA) supplemented with proteinase inhibitor cocktail (1:100 dilution; P8340; MilliporeSigma) and phosphatase inhibitor (1:100 dilution; P2850; MilliporeSigma). Proteins (30 μg/sample) were separated by electrophoresis on a 4–12% Bis-Tris Gel (NP0323BOX; Thermo Fisher Scientific) and then transferred to a nitrocellulose membrane with 0.4-μm pores. Antibodies used for Western blotting were anti-HMGCS2 antibody (clone EPR8642, ab137043; Abcam, Cambridge, MA, USA), anti-CBR2 antibody (ARP42461_P050; Aviva Systems Biology, San Diego, CA, USA), anti-β-tubulin antibody (clone BT76R, MA5-16308; Thermo Fisher Scientific).

ALI culture of primary tracheal epithelial cells

ALI culture was performed as described in You *et al.* (21). After overnight digestion of tracheas in pronase solution [0.15% w/v in membrane-thermotolerant *Escherichia coli* (mTEC) basic medium (DMEM and Ham's F-12) supplemented with 15 mM 4-(2-hydroxyethyl)-1-piperazineethanesulfonic acid, 4 mM L-glutamine, 3.6 mM $NaHCO_3$, 100 U/ml penicillin, and 100 mg/ml streptomycin], cells were seeded in collagen-coated cell inserts for 24-well plates. Cells were cultured for 7 d submerged in mTEC Plus buffer [mTEC basic medium supplemented with 10 mg/ml insulin, 5 mg/ml transferrin, 0.1 mg/ml cholera toxin, 25 ng/ml epidermal growth factor, 30 mg/ml bovine pituitary extract, and 5% fetal bovine serum (v/v)] to expend cell number. Then, cells were differentiated in air-liquid culture condition (no medium on top of the insert) with mTEC serum-free buffer (mTEC basic medium supplemented with 5 mg/ml insulin, 5 mg/ml transferrin, 0.025 mg/ml cholera toxin, 5 ng/ml epidermal growth factor, 30 mg/ml bovine pituitary extract, and 1 mg/ml bovine serum albumin) for 9 d to induce cilia genesis. Experiments were carried out in mixed male and female mice. At the end of the experiment, cells were fixed for immunofluorescence staining or frozen for RNA extraction.

Immunofluorescence

Frozen lung sections were stained with anti-CCSP antibody (07-623; MilliporeSigma) and Cy3 secondary antibody (CY-1300; Vector Laboratories, Burlingame, CA, USA). For cells grown in cell inserts, immunofluorescence staining was performed as described in Akram *et al.* (22) with the following antibodies: anti-acetylated tubulin (clone 6-11B-1, T7451-100UL; MilliporeSigma), anti-E–cadherin (clone 24E10, 3195s; Cell Signaling Technology, Danvers, MA, USA), goat anti-rabbit Alexa Fluor 488 (R37116; Thermo Fisher Scientific), and goat anti-mouse Cy3 (CY-1300; Vector Laboratories). All samples were stained with DAPI for nucleus and slides were mounted with VectaShield HardSet Antifade Mounting Medium (H1400; Vector Laboratories).

Adenovirus Cre-mediated *Bmal1* knockdown in primary tracheal cells and RNA-seq

The transfection was undertaken as described in Balasooriya *et al.* (23). High titer Ad5CMVCre virus (2×10^{e11} pfu/ml) was purchased from the Viral Vector Core Facility (University of Iowa, Iowa City, IA). After overnight culture of freshly isolated tracheal epithelial cells from *Bmal1*$^{f/f}$ mice, 0.5 μl virus solution was added into each well (~1000 pfu) with serum-free mTEC Plus solution. After 8 h, the virus medium was changed back to normal mTEC Plus medium and the cells were continually cultured as described above. For the *Bmal1* knockdown efficiency

www.fasebj.org by Oxford Univ Lib Serv - Bodleian Lib (163.1.203.50) on June 11, 2019. The FASEB Journal Vol. ${article.issue.getVolume()}, No. ${article.issue.getIssueNumber()}

study, cells differentiated in ALI condition were put into photomultiplier tubes to monitor Per2-luc activity after temperature synchronization [2 cycles of 12 h at 36.5°C and 12 h at 38.5°C (24)]. Two wells per unit of a 24-well plate were made in house to fit samples into the photomultiplier tubes. For time-serial RNA-seq, samples cultured at 37°C were collected after 2 d of temperature synchronization at 1 well per group per time point for 48 h. Poly(A) selected mRNA from 1 μg total RNA were used for RNA-seq in an Illumina HiSeq 4000 machine, with 12 samples per lane generating 75 × 75 base-pair end reads. The sequence data were analyzed as previously described except that rhythmic gene detection was carried out analyzing only the first cycle of RNA-seq data instead of 2 cycles of RNA-seq data due to weak gene oscillation *in vitro*. RNA-seq data were stored in Array Express (E-MTAB-6384).

Food entrainment and LPS challenge

C57BL/6 mice (males, 8–9-wk-old) were bought from Envigo. They were housed in normal condition initially for 1–2 wk before being kept in light-controlled cabinets. Mice were entrained to the light/dark cycle for 2 wk and then fed either on their day or night time for 2 wk before tissue collection or LPS treatment. In the cabinet, half ($n = 12$ in the first cohort and $n = 16$ in the second cohort) were maintained in the normal light/dark cycle (lights on at 7 AM and lights off at 7 PM), and the other half in reverse light/dark cycle (lights on at 7 PM and lights off at 7 AM). After 2 wk in the light/dark condition described above, restricted feeding was introduced. Mice were kept in the same light/dark condition with free access to water, and standard chow food was provided from 10 AM to 4 PM every day for 2 wk. In this way, half of the mice were fed in their subjective night and half were fed in their subjective day. Mice in cohort 1 were culled at the end of restricted feeding for lung tissue harvest. For mice in cohort 2, the aerosolized LPS exposure experiment was carried out at ZT0 (7 AM) and ZT12 (7 PM) ($n = 8$, feeding group/time point) as previously described in Gibbs *et al.* (11). BAL was collected with lung samples 5 h later. Cell count and fluorescence-activated cell-sorting analysis of BAL cells were performed as previously described. CXCL5 levels were measured with a CXCL5 ELISA Kit (DY254; Bio-Techne, Minneapolis, MN, USA), according to product protocol.

Quantitative PCR analysis

Total RNA (500 ng) was reverse transcribed into cDNA using an RNA to cDNA Kit (Thermo Fisher Scientific). Gene expression was studied by quantitative PCR (qPCR) in StepOnePlus machines (Thermo Fisher Scientific). The following Taqman gene expression assays were used: *Cxcl5* assay ID, Mm00436451_g1; *Cxcl15* assay, ID Mm00441243_m1; *Nr1d1* assay, ID Mm00520708_m1; and *Dbp* assay, ID Mm00497539_m1. *Snx31* and *18s* are studied by primers and a Roche Universal Probe (Basel, Switzerland) set as follows: *Snx31* forward primer 5′-AGATCTGGTGGGCTACTTCG-3′, reverse primer 5′-GTCGGCCAGCTTCTTCAC-3′, probe number 47; *18s* forward primer 5′-CTCAACACGGGAAACCTCAC-3′, reverse primer 5′-CGCTCCACCAACTAAGAACG-3′, probe number 77. Relative gene expression was calculated by δ C_t method with *18s* as housekeeping gene.

Statistics

Values are means ± SD. Data were analyzed using Prism v.5.0 (GraphPad Software, La Jolla, CA, USA). Unpaired Student's *t* tests (with Welch's corrections when variance was unequal) and 1- and 2-way ANOVAs were used, as appropriate. Significance was set at $P < 0.05$.

RESULTS

Background BAL neutrophilia, altered lung functions, and impaired influenza defense in *CCSP-Bmal1*$^{-/-}$ mice

Using flow cytometry, we analyzed BAL cells and identified significantly enhanced background neutrophilia in *CCSP-Bmal1*$^{-/-}$ mice (**Fig. 1*A*, *B***). Next, we assessed lung mechanical function by flexiVent in 4-mo-old mice, revealing elevated lung compliance (the measure of the ability of the lung to stretch and expand), reduced elastance [the reciprocal of compliance (*i.e.*, the pressure change that is required to elicit a unit volume change)] and a trend for reduced resistance of the respiratory tract to airflow. By 1 yr of age, these phenotypes were reversed in *CCSP-Bmal1*$^{-/-}$ mice (Fig. 1*C*–*E*). To test the potential involvement of changes to the extracellular matrix, we assessed collagen levels in the lung using picrosirius red staining. This revealed an increased collagen deposition in proximity to large airways of 1-yr-old mice (Fig. 1*F*). This indication of pulmonary scarring is the long-term consequence of increased neutrophil infiltration in *CCSP-Bmal1*$^{-/-}$ mouse lungs.

Our earlier studies have shown that *CCSP-Bmal1*$^{-/-}$ mice exhibit exaggerated acute inflammatory responses to LPS, mediated by abnormal regulation of selective chemokine signaling (11). To assess the generality of such responses, we adopted a chronic inflammatory model using an influenza challenge, which generates a strong local response in pulmonary tissues and damages airway epithelium, leading to a pattern of sustained inflammation with a well-defined time course over several days and weeks (25). Postinfection, we observed significantly greater weight loss in *CCSP-Bmal1*$^{-/-}$ mice over a 21-d course (Fig. 1*G*) but without an effect on mortality. This was confirmed in repeat experiments in which mice were culled on a single day (d 11 postinfection), and here histologic analysis revealed substantial regions of pulmonary consolidation in *CCSP-Bmal1*$^{-/-}$ mice compared with controls (Fig. 1*H* and Supplemental Fig. S1*C*). This was characterized by extensive T-cell marker CD3 immunofluorescence staining (Supplemental Fig. S1*A*), and, using a NanoString inflammatory gene array, we defined augmented expression of a number of chemokines and cytokines, including the lymphocyte attractant chemokine *Ccl20* (Supplemental Fig. S1*B*). Thus, *Bmal1* deletion in AECs imposes detrimental effects on both pulmonary homoeostasis and viral defense.

Genome-wide changes by time-series RNA-seq analysis in distal AECs from *CCSP-Bmal1*$^{-/-}$ and *Bmal1*$^{flox/flox}$ mice

Having established the importance of the circadian clock in AECs, we went on to study the global circadian transcriptome and effect of *Bmal1* deletion. To do this, we used

www.fasebj.org by Oxford Univ Lib Serv - Bodleian Lib (163.1.203.50) on June 11, 2019. The FASEB Journal Vol. ${article.issue.getVolume()}, No. ${article.issue.getIssueNumber()}

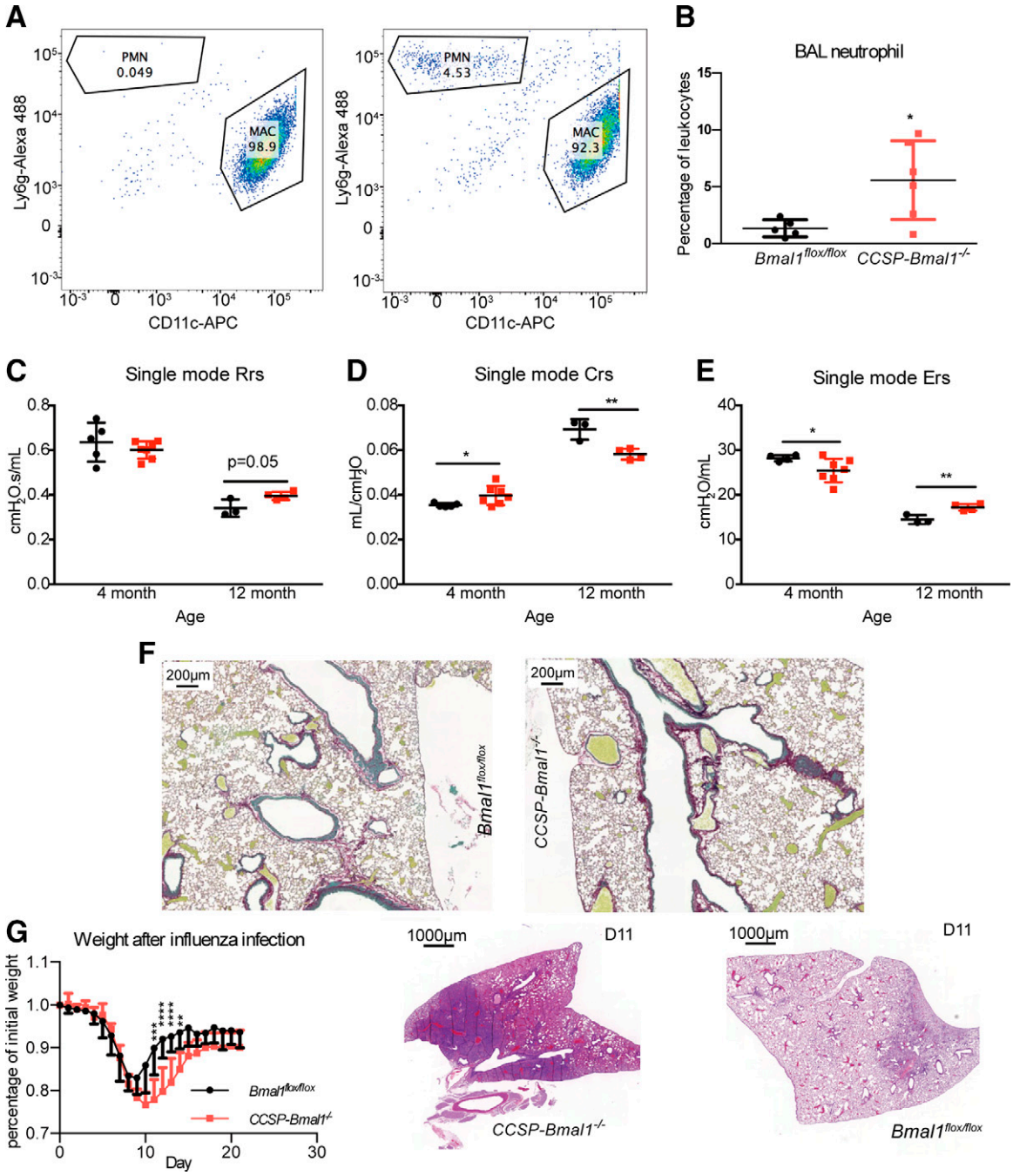

Figure 1. Altered pulmonary homeostasis and functions in *CCSP-Bmal1*$^{-/-}$ mice. BAL samples were collected in the morning from unchallenged young *CCSP-Bmal1*$^{-/-}$ and *Bmal1*$^{flox/flox}$ littermate controls for flow cytometry study. *A*) Flow cytometry plots for BAL macrophages and neutrophils from *Bmal1*$^{flox/flox}$ and *CCSP-Bmal1*$^{-/-}$ mice. *B*) BAL neutrophilia in *Bmal1*$^{flox/flox}$ and *CCSP-Bmal1*$^{-/-}$ mice. Data shown are means ± SD; Student's *t* test (n = 5–6/group). *$P < 0.05$. *C–E*) Measurement of lung biomechanical function in 4-mo-old and 12-mo-old *Bmal1*$^{flox/flox}$ and *CCSP-Bmal1*$^{-/-}$ mice assessed at ZT4–6. Rrs, lung resistance; Crs, lung compliance; and Ers, lung. Data shown are means ± SD; Student's *t* test between genotypes in the same age group (n = 5–7 in the 4-mo group, n = 3–4 in the 12-mo group). *$P < 0.05$, **$P < 0.01$. *F*) Examples of picrosirius red staining of larger airways in aged *CCSP-Bmal1*$^{-/-}$ and *Bmal1*$^{flox/flox}$ mice. *G*) Body weight changes over 21 d following influenza infection. Data shown are means ± SD; 2-way ANOVA with *post hoc* test (n = 5–6/group). **$P < 0.01$, ***$P < 0.001$, ****$P < 0.0001$. *H*) Example of lung hematoxylin and eosin staining 11 d postinfection.

LCM of distal AECs from frozen pulmonary sections, which allowed precise collections of targeted cells (CCSP-positive cells) from within intact tissue, without the alteration in cellular phenotypes associated with techniques such as flow cytometry. Staining of the AEC club cell marker CCSP showed strong enrichment in small airways (Supplemental Fig. S2*A*). The microdissected area is shown in Supplemental Fig. S2*B*, *C*. There was 5-fold enrichment in *Ccsp* mRNA levels of LCM-recovered cells compared with that in the whole lung (Supplemental Fig. S2*D*). Using animals maintained in constant darkness, we collected timed samples by LCM from AECs at 4 h

www.fasebj.org by Oxford Univ Lib Serv - Bodleian Lib (163.1.203.50) on June 11, 2019. The FASEB Journal Vol. ${article.issue.getVolume()}, No. ${article.issue.getIssueNumber()}

intervals over 2 circadian cycles (48 h). RNA-quality RNA and RNA-seq read-distribution was similar among samples (Supplemental Fig. S2*G*). Additionally, we compared gene transcript levels from RNA-seq at a single time point (CT8, 2 replicates per group) with those obtained by qPCR, and this revealed a near 1:1 concordance in expression (Supplemental Fig. S2*E*).

First, we examined core canonical circadian clock-regulating gene expression (**Fig. 2**). Strong circadian rhythms were observed in these genes from samples of *Bmal1*$^{flox/flox}$ mice. Among them, E-box– and D-box–regulated genes (*Tef*, *Chrono*, *Dbp*, *Nr1d1/Reverbα*, *Nr1d2/Reverbß*, *Per1*, *Per3*, *Dec1*, and *Dec2*) were all suppressed in the *CCSP-Bmal1*$^{-/-}$ group, compatible with the established direct action of *Bmal1* on these circadian elements. RAR-related orphan receptor element (RRE)–regulated transcripts (*Npas2*, *Cry1*, *Rorc*, *Nifl3/E4bp4*, and *Clock*) were all up-regulated in *CCSP-Bmal1*$^{-/-}$ group, compatible with the suppression of *Bmal1*-regulated *Reverb* expression, which normally represses RRE elements on these genes. A third group of genes showed little change, including *Hlf*, *Cry2*, *Rora*, and *Per2*, indicative of complex control *via* both E-box and RRE-regulating motifs and additional systemic cues. As an additional validation for potential cross-contamination with nontargeted cells, we examined RNA-seq read coverage over the floxed region (exon 8) of the *Bmal1* gene and showed that this region was deleted in all samples obtained from AECs of *CCSP-Bmal1*$^{-/-}$ mice (Supplemental Fig. S2*I*).

We used the MetaCycle meta2d function to identify circadian rhythmic transcripts. A total of 916 transcripts were detected as rhythmic in *Bmal1*$^{flox/flox}$ animals, which were nonrhythmic in *CCSP-Bmal1*$^{-/-}$ mice (**Fig. 3*A*** top panels, group 1). An additional set of 126 transcripts retained rhythmicity in both genotypes (Fig. 3*A*, middle panels, group 2). Unexpectedly, we also identified 856 transcripts that gained rhythmicity in *CCSP-Bmal1*$^{-/-}$ mice (Fig. 3*A*, bottom panels, group 3). This latter cohort of genes also exhibited a markedly different peak phase of expression compared with groups 1 and 2, displaced by ~9 h (Fig. 3*B*). Examples of genes in groups 1, 2, and 3 were shown in Supplemental Fig. S4*A*, with KEGG pathway

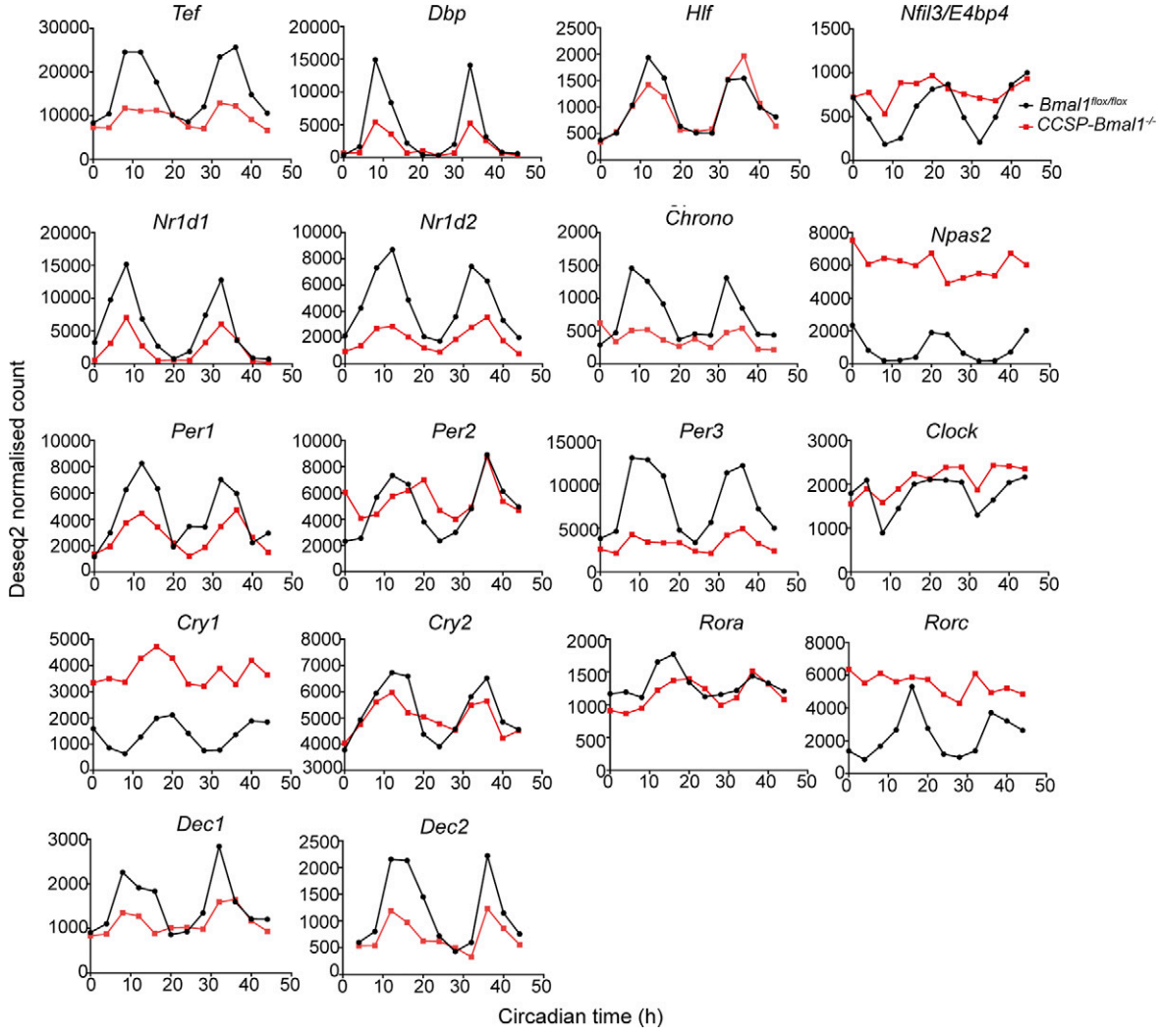

Figure 2. Disrupted core clock gene expression in *CCSP-Bmal1*$^{-/-}$ mice. Time-series (48 h) RNA-seq studies were carried out in LCM distal small AECs and RNA reads were normalized by DEseq2 method. Transcripts of core clock genes from *Bmal1*$^{flox/flox}$ (black solid circle) and *CCSP-Bmal1*$^{-/-}$ (red solid square) mice are shown. *Y*-axis labels DESeq2-normalized reads count, and *x*-axis labels CT.

www.fasebj.org by Oxford Univ Lib Serv - Bodleian Lib (163.1.203.50) on June 11, 2019. The FASEB Journal Vol. ${article.issue.getVolume()}, No. ${article.issue.getIssueNumber()}

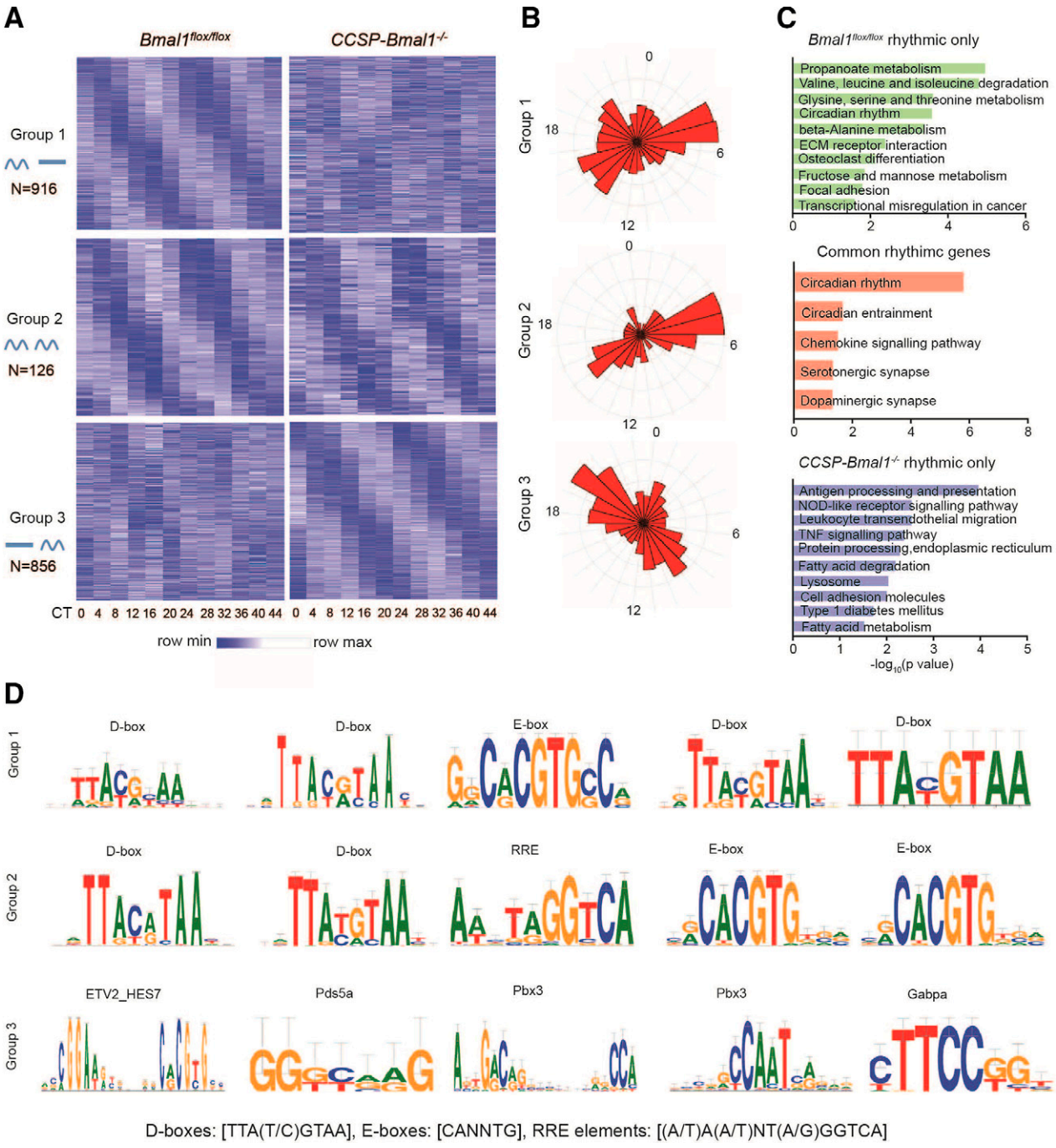

Figure 3. Circadian transcription in LCM distal AECs over 2 cycles. *A*) Group 1: rhythmically expressed transcripts in *Bmal1*$^{flox/flox}$ mice (left) compared with the same genes plotted for *CCSP-Bmal1*$^{-/-}$ mice (right). Group 2: common rhythmic genes in both genotypes. Group 3: newly emergent rhythmic transcripts in *CCSP-Bmal1*$^{-/-}$ mice (right) and expression of the same transcripts in *Bmal1*$^{flox/flox}$ group (left). *B*) Phase distribution of rhythmic genes of groups 1–3, which centers at CT5 and CT15 in groups 1 and 2, and at CT9 and CT20 in group 3. *C*) KEGG pathway enrichment analysis of genes in groups 1–3, ranked by significance, with most significant pathways as propionate metabolism in group 1, circadian rhythm in group 2, and antigen processing and presentation in group 3. *D*) Examples of enriched DNA motifs of rhythmic genes shown above in order of significance of fit.

enrichment (Fig. 3*C*). Relating to increased background neutrophilia phenotype, in addition to *Cxcl5*, both *Cxcl3* and *Cxcl15* were strongly rhythmic in *Bmal1*$^{flox/flox}$ AECs and highly increased in *CCSP-Bmal1*$^{-/-}$ samples. DNA motif enrichment analysis in gene-regulatory regions of rhythmic genes revealed dominant motifs resembling canonical circadian clock motifs D-boxes [TTA(T/C)GTAA], E-boxes (CANNTG), and RRE elements [(A/T)A(A/T)NT(A/G)GGTCA] for groups 1 and 2. In contrast, group 3 showed no enrichment for these circadian regulatory elements (Fig. 3*D*).

Rhythmic pathways were identified by different time of day in the lungs (Supplemental Fig. S3). The rhythmic pathways are largely different between genotypes (Supplemental Fig. S3*A*). In the common

www.fasebj.org by Oxford Univ Lib Serv - Bodleian Lib (163.1.203.50) on June 11, 2019. The FASEB Journal Vol. ${article.issue.getVolume()}, No. ${article.issue.getIssueNumber()}

rhythmic pathway, some show changed phases (Supplemental Fig. S3*B*). For example, the phase of metabolism of lipids and lipid proteins was shifted from CT18 in *Bmal*$^{flox/flox}$ mice to ~CT10 in *CCSP-Bmal1*$^{-/-}$ mice. Genotype-specific rhythmic pathways are shown in Supplemental Figs. S3*C*, *D*, most of which are in the daytime. In *Bmal1*$^{flox/flox}$ mice, pathways related to extracellular matrix are centered at early day, followed by pathways like pallet-activation signaling and aggregation, chemokine-signaling pathway in midday, and metabolism in the evening. In *CCSP-Bmal1*$^{-/-}$ mice, some of the rhythmic pathways are related to immune response, like antigen presentation and processing in early day.

Additionally, using DESeq2, we detected 814 transcripts with significantly increased (n = 507) or decreased (n = 307) expression across all time points in *CCSP-Bmal1*$^{-/-}$ mice, defined as DE. Of these, 642 were nonrhythmic in either genotype (**Fig. 4*A*, *B***). KEGG pathway analysis revealed enrichment in metabolism-related pathways and inflammatory pathways (Fig. 4*C*). Within the metabolic pathways, 20 of 82 genes were

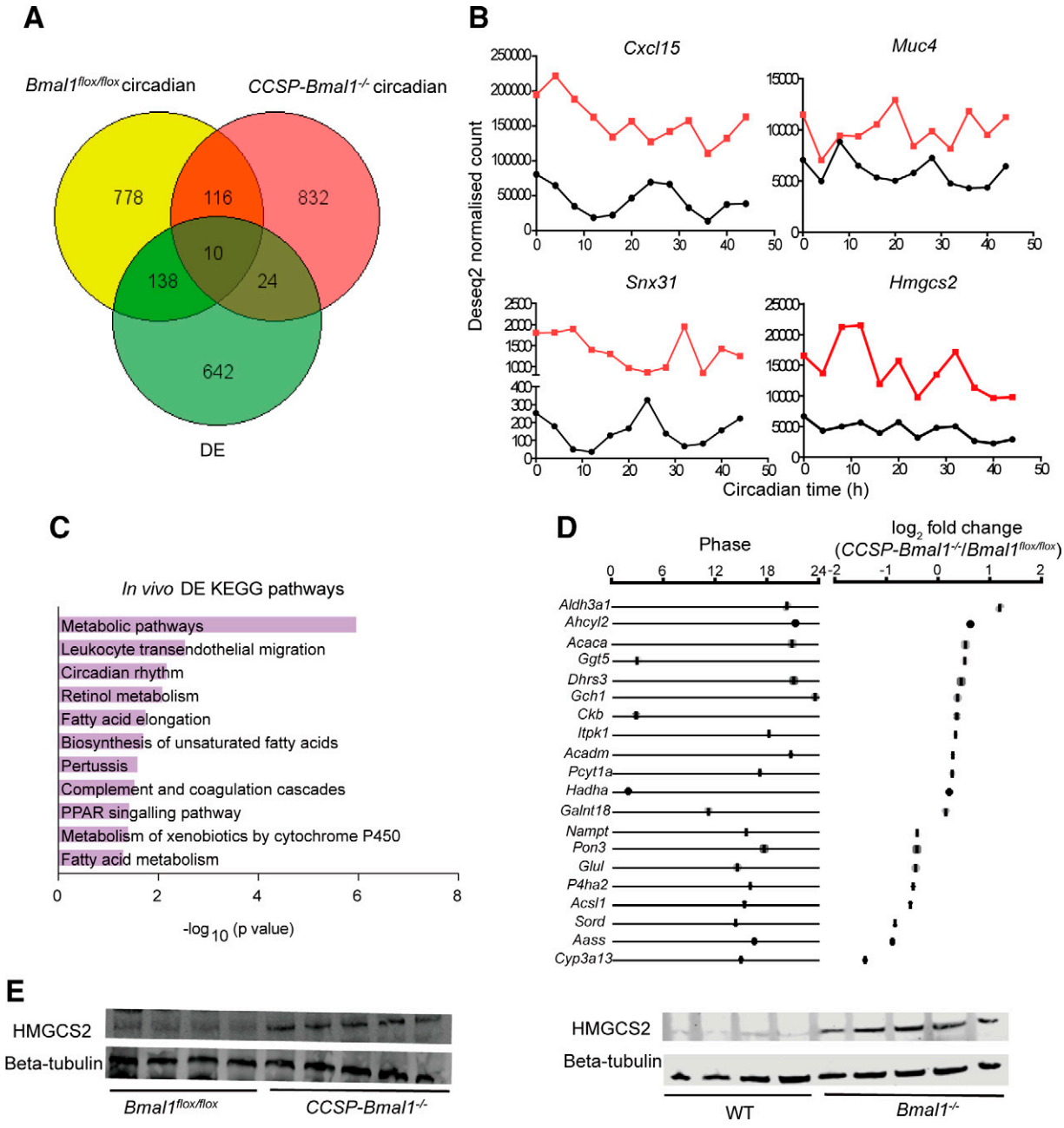

Figure 4. Analysis of metabolic-related DE gene sets in *Bmal1*-targeted cells. *A*) Overlap in expression of circadian gene sets from Fig. 3 with DE gene sets. *B*) Examples of 4 DE genes from *Bmal1*$^{flox/flox}$ (black solid circle) and *CCSP-Bmal1*$^{-/-}$ (red solid square). *C*) KEGG pathway enrichment analysis of DE genes, ranked in order of significance. *D*) Plots of phase and log2 fold changes of a subset of DE genes defined in metabolic pathways, which were rhythmic in *Bmal1*$^{flox/flox}$ group. *E*) HMGCS2 Western blots in whole-lung tissues from *CCSP-Bmal1*$^{-/-}$ (left) and global *Bmal1*$^{-/-}$ (right) mice. Samples were taken at ZT4. Each lane contained a single sample.

www.fasebj.org by Oxford Univ Lib Serv - Bodleian Lib (163.1.203.50) on June 11, 2019. The FASEB Journal Vol. ${article.issue.getVolume()}, No. ${article.issue.getIssueNumber()}

rhythmic in *Bmal1*$^{flox/flox}$ samples, with a range of peak phases in expression (CT12-24, Fig. 4*D*). Increased *Hmgcs2* expression was validated by Western blotting, showing strong induction of a gene in the lungs of both *CCSP-Bmal1*$^{-/-}$ mice and in mice bearing a global deletion of *Bmal1* (*Bmal1*$^{-/-}$; Fig. 4*E* and Supplemental Fig. S4*B*), the expression of which is normally restricted to the liver and gut (26), indicating an impact on differentiated cell function.

Thus, *Bmal1* disruption leads to not only widespread impact on metabolic and inflammatory pathways in AECs but also the striking emergence of an additional novel rhythmic transcriptome in targeted cells.

Cell-autonomous effect of *Bmal1* in ALI differentiated primary tracheal cells *in vitro*

Given the importance of cellular communication *in vivo*, it is crucial to address the question of whether the effect of *Bmal1* in AEC clockwork is cell-autonomous or is regulated by local pulmonary signals. For this purpose, we adopted an *in vitro* ALI model to culture primary pulmonary tracheal epithelial cells derived from *Bmal1*$^{-/-}$ knockout mice and wild-type (WT) littermate mice. The ALI model is widely regarded as a gold standard for the study of primary airway epithelia. In both genotypes, we observed clear development of characteristic-ciliated cells (**Fig. 5*A–D***), and chemokines previously shown as

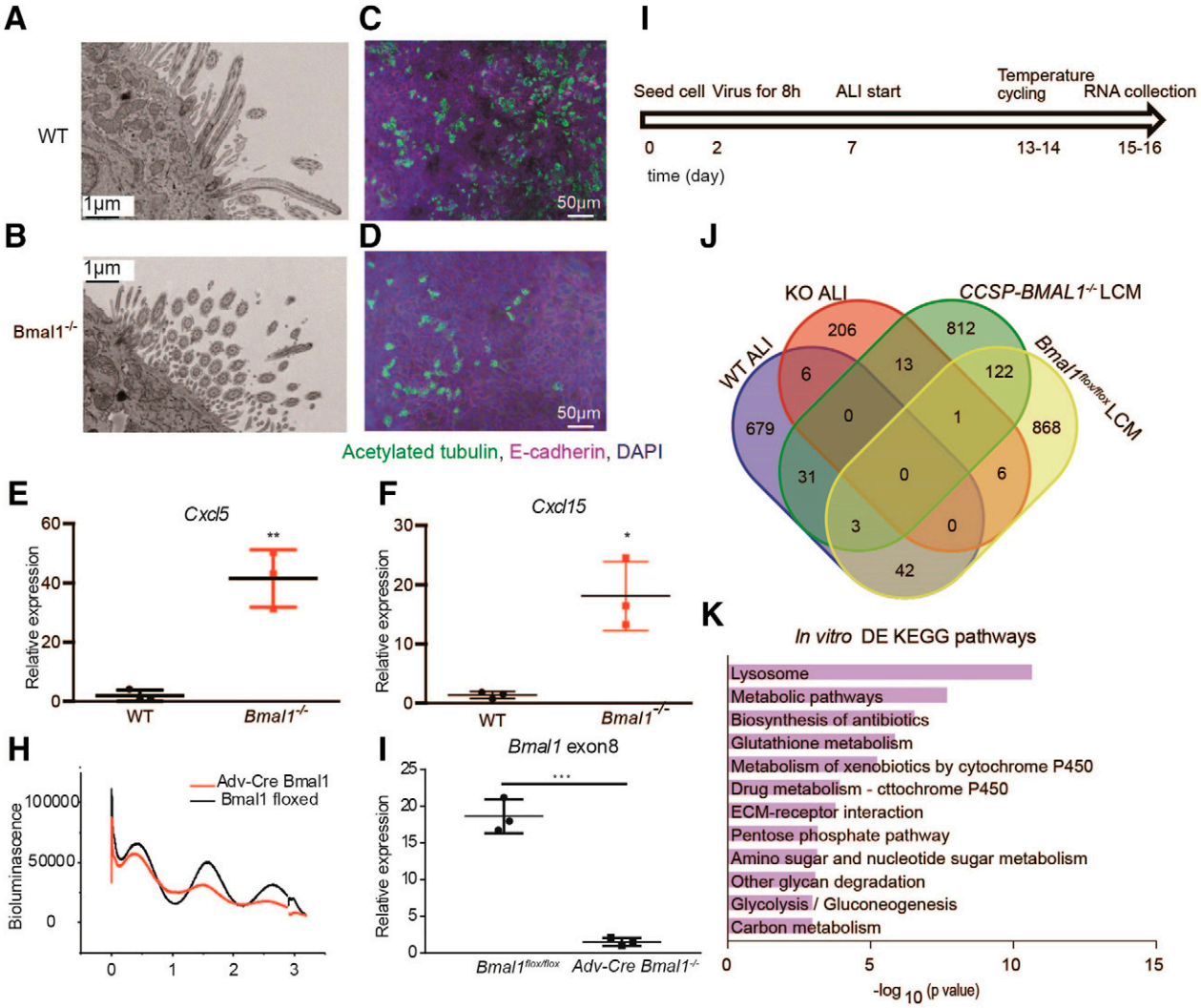

Figure 5. Cell-autonomous *Bmal1* function in ALI culture of primary mouse tracheal cells. ALI cultures were established using primary tracheal epithelial cells from WT and global *Bmal1*$^{-/-}$ mice, with 7 d under submerged condition and another 10 d exposed to air in the apical side of cells. *A*, *B*) Electron microscopy images for cilia in ALI primary tracheal cells from WT and global *Bmal1*$^{-/-}$ mice, respectively. *C*, *D*) Immunofluorescence staining of cilia markers (acetylated tubulin) and epithelial cell markers (E-cadherin) in ALI primary tracheal cells from WT and global Bmal1$^{-/-}$ mice, respectively. *E*, *F*) *Cxcl5* and *Cxcl15* gene expression measurement by qPCR in ALI primary tracheal cells from WT and global *Bmal1*$^{-/-}$ mice. Data shown are means ± SD; Student's *t* test ($n = 3$/genotype). $^*P < 0.05$, $^{**}P < 0.01$. *G*) Expression of *Bmal1* exon 8 in primary tracheal cells 2 d after infection. Data shown are means ± SD; Student's *t* test ($n = 3$/genotype). $^{***}P < 0.001$. *H*) Bioluminescence traces of *Per2-luc* in control and Adv-Cre–transfected ALI primary tracheal cells 21 d in culture. *I*) Schematic description of viral Cre infection in primary tracheal cells from *Bmal1*$^{flox/flox}$ mice. *J*) Overlap of expression of rhythmic genes during ALI culture and LCM studies. *K*) KEGG pathway enrichment of DE genes in cell culture study. Pathways are ranked by significance value.

www.fasebj.org by Oxford Univ Lib Serv - Bodleian Lib (163.1.203.50) on June 11, 2019. The FASEB Journal Vol. ${article.issue.getVolume()}, No. ${article.issue.getIssueNumber()}

abnormally regulated *in vivo* in *CCSP-Bmal1*$^{-/-}$ mice were also significantly augmented by 20–40 folds in long-term cultured AECs (Fig. 5*E, F*). Thus, dysregulation of chemokine pathways operates in a cell-intrinsic manner upon *Bmal1* deletion. In order to exclude potential contributions arising from tissue-wide reprogramming effects of cells derived from *Bmal1*-null mice (27), we next cultured AECs from *Bmal1*$^{flox/flox}$ mice on a PER2::LUC reporter background and treated these cells with an adenovirus-expressing Cre driven by cytomegalovirus promoter, leading to loss of exon 8 in targeted cells (Fig. 5*G*). We confirmed the efficiency of targeting by tracking PER2::LUC bioluminescence 2 wk after infection, revealing initial dampening and subsequent loss of overt circadian rhythmicity (Fig. 5*H*).

To define the impact on circadian-regulated pathways, AECs were seeded, Cre-transfected, and cultured in ALI for 7 d; then, cells were subjected to circadian temperature synchronization for 2 d, and subsequently RNA was collected every 4 h for 48 h (Fig. 5*I*). RNA-seq revealed 762 rhythmic transcripts in *Bmal1*$^{flox/flox}$ cells, with 232 transcripts in Cre-transfected cells, only 6 of which were common to both data sets (Fig. 5*J*). Pathway enrichment of rhythmic genes in control cells revealed a strikingly consistent pattern with that observed in LCM-derived *Bmal1*$^{-/-}$ AECs from whole lung (Supplemental Fig. S5 compared with Fig. 3*C*). Interestingly, despite the close similarity of cellular processes, the specific transcriptional composition of these 2 data sets showed relatively little overlap (Fig. 5*J*). Additionally, a total of 3041 genes showed significantly altered expression (Supplemental Fig. S6 and Supplemental Data) in which pathway analysis revealed common signatures in these data sets (Fig. 5*K vs.* Fig. 4C). These common elements included circadian clock- and chemokine-regulating genes (Supplemental Fig. S6).

Feeding is the zeitgeber of lung inflammatory response

The above studies indicate an important role for AEC circadian clock in regulating physiology, the emergence of a novel rhythmic transcriptome in *Bmal1*-deleted AECs *in vivo*, and the cell-autonomous nature of *Bmal1* effect. But this leaves the unanswered issue of how the pulmonary clockwork may be entrained. Recent studies have highlighted the importance of systemic metabolic cues in entraining peripheral oscillators and, in particular, the role of timed feeding (28). We therefore examined the role of timed feeding cues on the circadian-gated pulmonary inflammatory response to LPS (**Fig. 6*A***). Restriction of feeding to the light phase reversed the phase of expression of circadian clock genes like *Nr1d1* and *Dbp* in the lung (Fig. 6*B, C*). We also assessed *Bmal1* target genes such as *Snx31*, which also showed significant phase reversal in expression (Fig. 6*D*). We then tested the circadian gating mechanism driving pulmonary inflammatory responses to LPS (11). Night-fed mice treated with aerosolized LPS showed significantly higher inflammatory responses at ZT0 than ZT12, exhibited by higher numbers of BAL-total leukocyte, neutrophil infiltration, and CXCL5 levels. This is compatible with our earlier studies, with peak responses during the circadian daytime in mice (11). In contrast, mice confined to feeding during the day exhibited a clear phase reversal of inflammatory parameters (Fig. 6*E–G*). Thus, feeding cues act as a potent local synchronizing factor (ZT) in entraining

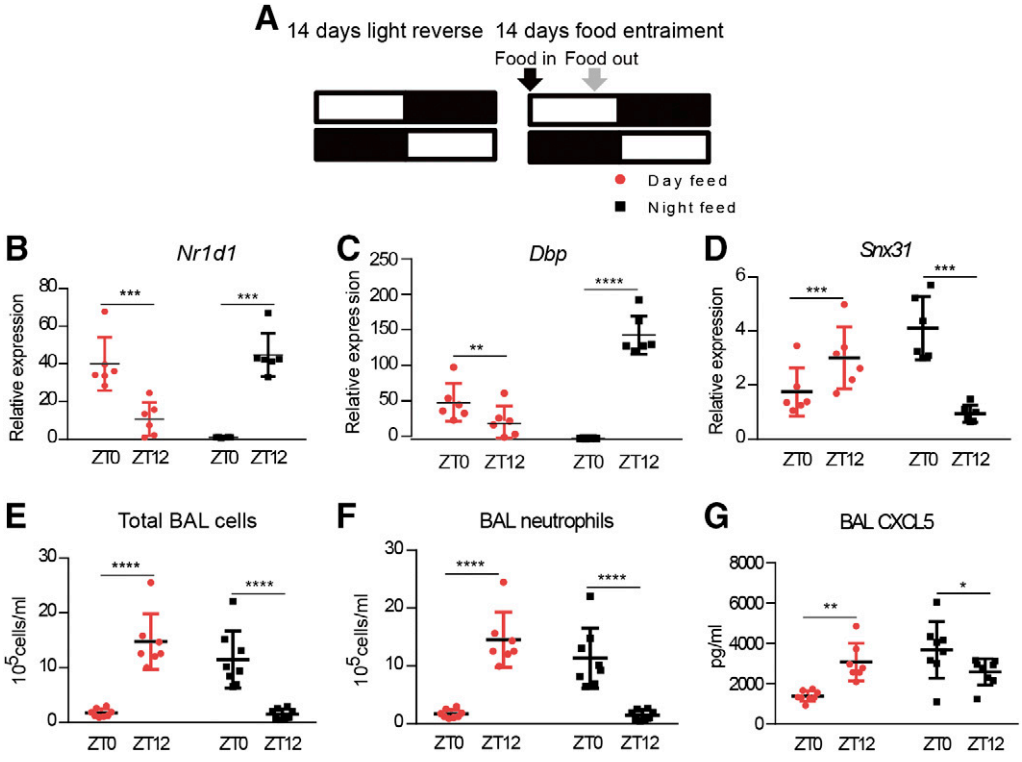

Figure 6. Reverse feeding resets time of day variation in pulmonary LPS response. *A*) Schematic description of experiment design. The food-reversal experiment was undertaken using 2 separate cohorts. *B–D*) Food reversal without LPS treatment was performed in cohort 1. *E–G*) Aerosolized LPS exposure experiment at ZT0 *vs.* ZT12 was performed in cohort 2 and total BAL cells, neutrophils, and CXCL5 concentrations measured. Gene expression was determined in cohort 2. Data analyzed by 2-way ANOVA with *post hoc* test to examine time of day difference within genotypes (n = 6–8). $^*P < 0.05$, $^{**}P < 0.01$, $^{***}P < 0.001$, $^{****}P < 0.0001$ (significant time of day difference within genotypes).

www.fasebj.org by Oxford Univ Lib Serv - Bodleian Lib (163.1.203.50) on June 11, 2019. The FASEB Journal Vol. ${article.issue.getVolume()}, No. ${article.issue.getIssueNumber()}

circadian-regulated pathways in the lung and circadian gating of responses to inflammatory stimuli.

DISCUSSION

Here we show that *Bmal1* plays an important role in a diverse range of cellular functions in AECs, regulating pulmonary neutrophil infiltration, biomechanical function, and influenza infection. Further, we show that the AEC clockwork retains a markedly autonomous phenotype in culture. Key findings are summarized in illustration **Fig. 7**. Our earlier studies have shown an important role for *Bmal1* in AECs in the circadian gating of LPS-induced pulmonary inflammation (11), whereas other groups using the global *Bmal1* knockout have described broadly similar pulmonary phenotypes, including an elevated pulmonary neutrophilia (7), aberrant responses to chronic inflammatory stimuli (8, 9), and impaired mechanical function (29). We now show the pulmonary AEC is the critical cell type in mediating these effects.

Time-series analysis of laser-captured AECs revealed widespread disruption in the complex of canonical core clock genes in *Bmal1*-targeted cells, similar in directions to findings in liver and adipose tissue (30, 31). We also identified a subset of rhythmic genes common to both WT and *Bmal1*-targeted AECs (group 2), with a similar phase angle for peak expression. These could be generated by systemic cues, 1 example of which is a glucocorticoid-induced gene *Gilz* (Supplemental Fig. S3). Interestingly, a substantial number of emergent rhythmic transcripts were detected in *Bmal1*-deleted mice (group 3), with a marked difference in phase angle. KEGG analysis of this latter data set revealed the emergence of pathways predominantly controlling immune responses, but this was not associated with migration of leukocytes to the pulmonary epithelium in *Bmal1*-deficient mice. Here, motif analysis revealed no significant enrichment of canonical circadian regulatory motifs. Remarkably, although disruption of *Bmal1* in AECs impacted a significant proportion of the expressed transcriptome, overall there was relatively little change in the total proportion of rhythmic transcripts due to the emergence of novel rhythmic transcripts in targeted cells. This counterintuitive outcome is also consistent with

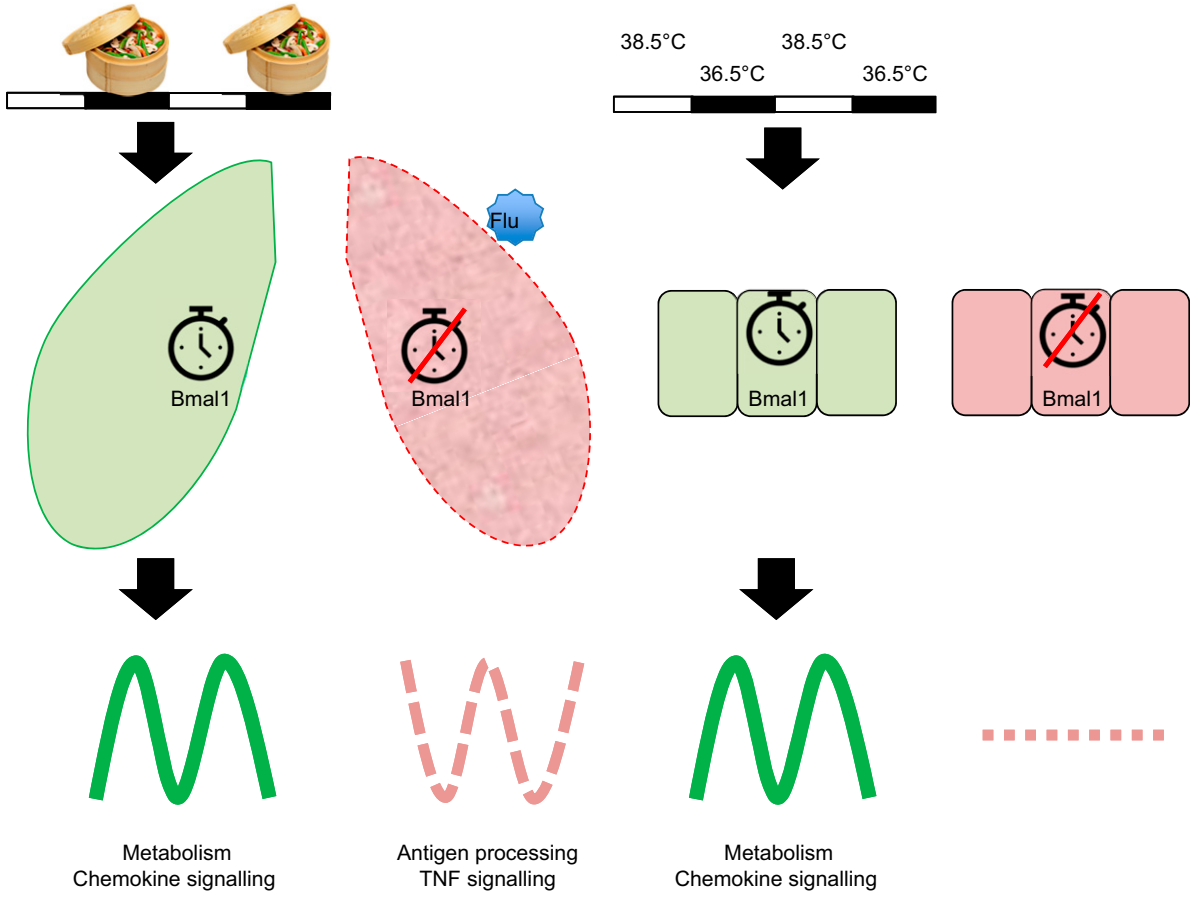

Figure 7. Illustration of key findings. Feeding sets the time of lung *in vivo*, driving rhythmic expression of core clock proteins like BMAL1 and more widespread rhythmic genes in club cells, involving mainly metabolic- and chemokine-signaling pathways. Deletion of *Bmal1* in club cells abolishes these rhythmically expressed genes and uncovers a different set of newly rhythmic genes. This may be due to other rhythmic signals *in vivo*. *CCSP-Bmal1*$^{-/-}$ mice show altered lung mechanic functions and more severe influenza infection. *In vitro*, primary AECs were able to generate rhythmic gene expression under temperature entrainment, and deletion of *Bmal1* disrupts genome-wide rhythmic gene expression without generating newly rhythmic gene expression. Flu stands for influenza in the picture.

www.fasebj.org by Oxford Univ Lib Serv - Bodleian Lib (163.1.203.50) on June 11, 2019. The FASEB Journal Vol. ${article.issue.getVolume()}, No. ${article.issue.getIssueNumber()}

studies of the mouse liver in which *Bmal1* is disrupted or during aging (32, 33) and suggests that a hitherto unrecognized feature of the endogenous cellular clockwork may be the ability to mask exogenous rhythmic signals from adjacent cells and tissues.

The mechanisms involved in synchronization of peripheral tissue and rhythmic physiologic responses still remain very poorly understood (4). However, a number of studies have highlighted the importance of metabolic-associated cues and that restriction of feeding to abnormal circadian phases in mice is sufficient to phase-shift transcriptional rhythms of peripheral tissue (28). With a similar protocol, we showed clear phase reversal for expression of core clock-regulating genes, as well as matrix-associated and chemokine genes. This protocol reset the circadian gating mechanism driving endotoxin responses, with a 12 h phase-shift in feeding time–reversed mice. This implicates metabolic cues as important general regulators of rhythmic immunity. The clear translational implication is that timing of feeding should be considered in clinical studies of circadian pulmonary function (34).

A critical question is whether the transcriptional changes seen in targeted AECs arise as a consequence of cell-intrinsic *Bmal1* function or because of the exposure of resident AECs to multiple extrinsic signals from neighboring cells and systemic cues. We tested this by using a cell culture model. This revealed strongly rhythmic expression for chemokine genes (*e.g.*, *Cxcl5*), with loss of clock control and up-regulation in *Bmal1*-disrupted cells, phenocopying the situation in intact tissues (11). Further RNA-seq profiling and subsequent pathway analyses revealed a consistent and comparable enrichment of common pathways with those identified in laser-captured cells from whole lung and previous studies of whole-lung tissues (35). Processes involved in metabolism, xenobiotic detoxification, chemokine signaling, and extracellular matrix dominated these. Strikingly, despite the similarity of function, there was relatively little overlap of specific gene sets in our cell culture studies with those from laser-captured cells, possibly reflecting differences in gene expression between small and large airway structures (36). Our data therefore show that many of the critical functions of *Bmal1* in pulmonary epithelial cells are cell-intrinsic and not indirectly regulated by extrinsic factors.

Our approaches here employed LCM as a means to isolate pulmonary small airway cells. Such dissection does not allow fine-scale resolution to cellular subtypes, nor can we attribute high-resolution cell-specific phenotypes in *ex vivo* culture models. For this, single-cell imaging approaches could be used to allow dynamical assessment of individual gene products, currently an unrealized gold standard in the field. However, use of LCM does allow the instantaneous assessment of the state of specific cells from primary tissues, without concerns associated with cell sorting and subsequent phenotypical drift. Nonetheless, an impressive feature of our data is the persistence of primary phenotypes in cultured AECs.

In summary, we reveal that the circadian circuitry within the pulmonary AEC is essential for pulmonary physiology and immunity, the main functions of which were under circadian control (Fig. 7). An AEC-specific circadian transcriptome was revealed, as well as the effect of *Bmal1* deletion, both *in vivo* and *in vitro*. *Bmal1* regulation operates in a cell-intrinsic manner, and circadian clock in the lung is synchronized by metabolic feeding-associated cues. Collectively, this work has implications for the role of the clock in multiple pulmonary diseases such as cancer, asthma, and chronic obstructive pulmonary disease, in which the circadian clockwork is commonly disrupted. FJ

ACKNOWLEDGMENTS

The authors thank Ian Donaldson and Andy Hayes (Bioinformatics and Genomic Technologies Core Facilities, University of Manchester) for providing support with regard to chromatin immunoprecipitation sequencint (ChIP) and RNA-seq analysis and sequencing, Dr. Halina Dobrzynski and Garry Ashton (University of Manchester) for access to LCM machines, Prof. Colin Bingle's group (University of Sheffield, Sheffield, England) in the training of primary AEC ALI culture, Dr. Emma Rawlins (University of Cambridge, Cambridge, United Kingdom) for communications of the Cre virus transfection method, Dr. Christoph Ballestrem, Rachel Lennon, and Patrick Caswell (all from the University of Manchester) for discussions of epithelial cell biology, the Genomics Center for RNA-seq Service, the Histology Laboratory, and Bioimaging Facility, University of Manchester for tissue section studies, and members of the laboratories of A.S.I.L. and D.W.R. for general discussions. The work is supported by Biotechnology and Biological Sciences Research Council (BBSRC) grants awarded to A.S.I.L. and D.W.R. (BB/L000954/1 and BB/K003097/1). D.W.R. and A.S.I.L. are Wellcome Investigators (Wellcome Trust; 107849/Z/15/Z). J.B.H. is supported by the U.S. National Institutes of Health, National Institute of Neurological Disorders and Stroke (2R01NS054794 to J.B.H. and A.S.I.L.). The authors declare no conflicts of interest.

AUTHOR CONTRIBUTIONS

Z. Zhang, D. W. Ray, and A. S. I. Loudon developed the concept and wrote the manuscript; Z. Zhang designed and performed the experiments; T. Hopwood, J. F. Blaikley, M. Rattray, J. B. Hogenesch, and J. Gibbs helped with experiment design; L. Hunter, G. Wu, R. Maidstone, Y. Mizoro, and P. Wang helped analysis of RNA-seq data; M. Fife helped performing influenza experiment; P. Cunningham and H. Durrington helped with lung function study; and N. Begley, B. Saer, M. Baxter, and T. Hussell helped with reverse feeding experiment.

REFERENCES

1. Takahashi, J. S. (2017) Transcriptional architecture of the mammalian circadian clock. *Nat. Rev. Genet.* **18**, 164–179
2. Kondratov, R. V., Kondratova, A. A., Gorbacheva, V. Y., Vykhovanets, O. V., and Antoch, M. P. (2006) Early aging and age-related pathologies in mice deficient in BMAL1, the core componentof the circadian clock. *Genes Dev.* **20**, 1868–1873
3. Bunger, M. K., Wilsbacher, L. D., Moran, S. M., Clendenin, C., Radcliffe, L. A., Hogenesch, J. B., Simon, M. C., Takahashi, J. S., and Bradfield, C. A. (2000) Mop3 is an essential component of the master circadian pacemaker in mammals. *Cell* **103**, 1009–1017
4. Bass, J., and Lazar, M. A. (2016) Circadian time signatures of fitness and disease. *Science* **354**, 994–999
5. Papagiannakopoulos, T., Bauer, M. R., Davidson, S. M., Heimann, M., Subbaraj, L., Bhutkar, A., Bartlebaugh, J., Vander Heiden, M. G., and

www.fasebj.org by Oxford Univ Lib Serv - Bodleian Lib (163.1.203.50) on June 11, 2019. The FASEB Journal Vol. ${article.issue.getVolume()}, No. ${article.issue.getIssueNumber()}

Jacks, T. (2016) Circadian rhythm disruption promotes lung tumorigenesis. *Cell Metab.* **24**, 324–331
6. Pekovic-Vaughan, V., Gibbs, J., Yoshitane, H., Yang, N., Pathiranage, D., Guo, B., Sagami, A., Taguchi, K., Bechtold, D., Loudon, A., Yamamoto, M., Chan, J., van der Horst, G. T., Fukada, Y., and Meng, Q. J. (2014) The circadian clock regulates rhythmic activation of the NRF2/glutathione-mediated antioxidant defense pathway to modulate pulmonary fibrosis. *Genes Dev.* **28**, 548–560
7. Haspel, J. A., Chettimada, S., Shaik, R. S., Chu, J. H., Raby, B. A., Cernadas, M., Carey, V., Process, V., Hunninghake, G. M., Ifedigbo, E., Lederer, J. A., Englert, J., Pelton, A., Coronata, A., Fredenburgh, L. E., and Choi, A. M. K. (2014) Circadian rhythm reprogramming during lung inflammation. *Nat. Commun.* **5**, 4753
8. Ehlers, A., Xie, W., Agapov, E., Brown, S., Steinberg, D., Tidwell, R., Sajol, G., Schutz, R., Weaver, R., Yu, H., Castro, M., Bacharier, L. B., Wang, X., Holtzman, M. J., and Haspel, J. A. (2018) BMAL1 links the circadian clock to viral airway pathology and asthma phenotypes. *Mucosal Immunol.* **11**:97–111
9. Edgar, R. S., Stangherlin, A., Nagy, A. D., Nicoll, M. P., Efstathiou, S., O'Neill, J. S., and Reddy, A. B. (2016) Cell autonomous regulation of herpes and influenza virus infection by the circadian clock. *Proc. Natl. Acad. Sci. USA* **113**, 10085–10090
10. Hwang, J. W., Sundar, I. K., Yao, H., Sellix, M. T., and Rahman, I. (2014) Circadian clock function is disrupted by environmental tobacco/cigarette smoke, leading to lung inflammation and injury via a SIRT1-BMAL1 pathway. *FASEB J.* **28**, 176–194
11. Gibbs, J., Ince, L., Matthews, L., Mei, J., Bell, T., Yang, N., Saer, B., Begley, N., Poolman, T., Pariollaud, M., Farrow, S., DeMayo, F., Hussell, T., Worthen, G. S., Ray, D., and Loudon, A. (2014) An epithelial circadian clock controls pulmonary inflammation and glucocorticoid action. *Nat. Med.* **20**, 919–926
12. Bayes, H. K., Ritchie, N., Irvine, S., and Evans, T. J. (2016) A murine model of early Pseudomonas aeruginosa lung disease with transition to chronic infection. *Sci. Rep.* **6**, 35838
13. Betsuyaku, T., and Senior, R. M. (2004) Laser capture microdissection and mRNA characterization of mouse airway epithelium: methodological considerations. *Micron* **35**, 229–234
14. Love, M. I., Huber, W., and Anders, S. (2014) Moderated estimation of fold change and dispersion for RNA-seq data with DESeq2. *Genome Biol.* **15**, 550
15. Wu, G., Anafi, R. C., Hughes, M. E., Kornacker, K., and Hogenesch, J. B. (2016) MetaCycle: an integrated R package to evaluate periodicity in large scale data. *Bioinformatics* **32**, 3351–3353
16. Huang, W., Sherman, B. T., and Lempicki, R. A. (2009) Bioinformatics enrichment tools: paths toward the comprehensive functional analysis of large gene lists. *Nucleic Acids Res.* **37**, 1–13
17. Huang, D. W., Sherman, B. T., Tan, Q., Kir, J., Liu, D., Bryant, D., Guo, Y., Stephens, R., Baseler, M. W., Lane, H. C., and Lempicki, R. A. (2007) DAVID bioinformatics resources: expanded annotation database and novel algorithms to better extract biology from large gene lists. *Nucleic Acids Res.* **35**,W169–W175
18. Kuleshov, M. V., Jones, M. R., Rouillard, A. D., Fernandez, N. F., Duan, Q., Wang, Z., Koplev, S., Jenkins, S. L., Jagodnik, K. M., Lachmann, A., McDermott, M. G., Monteiro, C. D., Gundersen, G. W., and Ma'ayan, A. (2016) Enrichr: a comprehensive gene set enrichment analysis web server 2016 update. *Nucleic Acids Res.* **44**, W90–W97
19. Chen, E. Y., Tan, C. M., Kou, Y., Duan, Q., Wang, Z., Meirelles, G. V., Clark, N. R., and Ma'ayan, A. (2013) Enrichr: interactive and collaborative HTML5 gene list enrichment analysis tool. *BMC Bioinformatics* **14**, 128
20. Zhang, R., Podtelezhnikov, A. A., Hogenesch, J. B., and Anafi, R. C. (2016) Discovering biology in periodic data through phase set enrichment analysis (PSEA). *J. Biol. Rhythms* **31**, 244–257
21. You, Y., and Brody, S. L. (2013) Culture and differentiation of mouse tracheal epithelial cells. *Methods Mol. Biol.* **945**, 123–143
22. Akram, K. M., Moyo, N. A., Leeming, G. H., Bingle, L., Jasim, S., Hussain, S., Schorlemmer, A., Kipar, A., Digard, P., Tripp, R. A., Shohet, R. V., Bingle, C. D., and Stewart, J. P. (2018) An innate defense peptide BPIFA1/SPLUNC1 restricts influenza A virus infection. *Mucosal Immunol.* **11**, 71–81; erratum: 1008
23. Balasooriya, G. I., Johnson, J. A., Basson, M. A., and Rawlins, E. L. (2016) An FGFR1-SPRY2 signaling axis limits basal cell proliferation in the steady-state airway epithelium. *Dev. Cell* **37**, 85–97
24. Saini, C., Morf, J., Stratmann, M., Gos, P., and Schibler, U. (2012) Simulated body temperature rhythms reveal the phase-shifting behavior and plasticity of mammalian circadian oscillators. *Genes Dev.* **26**, 567–580
25. Gregory, D. J., and Kobzik, L. (2015) Influenza lung injury: mechanisms and therapeutic opportunities. *Am. J. Physiol. Lung Cell. Mol. Physiol.* **309**, L1041–L1046
26. Puchalska, P., and Crawford, P. A. (2017) Multi-dimensional roles of ketone bodies in fuel metabolism, signaling, and therapeutics. *Cell Metab.* **25**, 262–284
27. Yang, G., Chen, L., Grant, G. R., Paschos, G., Song, W. L., Musiek, E. S., Lee, V., McLoughlin, S. C., Grosser, T., Cotsarelis, G., and FitzGerald, G. A. (2016) Timing of expression of the core clock gene Bmal1 influences its effects on aging and survival. *Sci. Transl. Med.* **8**, 324ra16
28. Ramkisoensing, A., and Meijer, J. H. (2015) Synchronization of biological clock neurons by light and peripheral feedback systems promotes circadian rhythms and health. *Front. Neurol.* **6**, 128
29. Sundar, I. K., Ahmad, T., Yao, H., Hwang, J. W., Gerloff, J., Lawrence, B. P., Sellix, M. T., and Rahman, I. (2015) Influenza A virus-dependent remodeling of pulmonary clock function in a mouse model of COPD. *Sci. Rep.* **4**, 9927
30. Liu, A. C., Tran, H. G., Zhang, E. E., Priest, A. A., Welsh, D. K., and Kay, S. A. (2008) Redundant function of REV-ERBalpha and beta and non-essential role for Bmal1 cycling in transcriptional regulation of intracellular circadian rhythms. *PLoS Genet.* **4**, e1000023
31. Paschos, G. K., Ibrahim, S., Song, W. L., Kunieda, T., Grant, G., Reyes, T. M., Bradfield, C. A., Vaughan, C. H., Eiden, M., Masoodi, M., Griffin, J. L., Wang, F., Lawson, J. A., and Fitzgerald, G. A. (2012) Obesity in mice with adipocyte-specific deletion of clock component Arntl. *Nat. Med.* **18**, 1768–1777
32. Atger, F., Gobet, C., Marquis, J., Martin, E., Wang, J., Weger, B., Lefebvre, G., Descombes, P., Naef, F., and Gachon, F. (2015) Circadian and feeding rhythms differentially affect rhythmic mRNA transcription and translation in mouse liver. *Proc. Natl. Acad. Sci. USA* **112**, E6579–E6588
33. Sato, S., Solanas, G., Peixoto, F. O., Bee, L., Symeonidi, A., Schmidt, M. S., Brenner, C., Masri, S., Benitah, S. A., and Sassone-Corsi, P. (2017) Circadian reprogramming in the liver identifies metabolic pathways of aging. *Cell* **170**, 664–677.e11
34. Anafi, R. C., Francey, L. J., Hogenesch, J. B., and Kim, J. (2017) CYCLOPS reveals human transcriptional rhythms in health and disease. *Proc. Natl. Acad. Sci. USA* **114**, 5312–5317
35. Sukumaran, S., Jusko, W. J., Dubois, D. C., and Almon, R. R. (2011) Light-dark oscillations in the lung transcriptome: implications for lung homeostasis, repair, metabolism, disease, and drug action. *J. Appl. Physiol.* **110**, 1732–1747
36. Zuo, W., Zhang, T., Wu, D. Z., Guan, S. P., Liew, A. A., Yamamoto, Y., Wang, X., Lim, S. J., Vincent, M., Lessard, M., Crum, C. P., Xian, W., and McKeon, F. (2015) p63(+)Krt5(+) distal airway stem cells are essential for lung regeneration. *Nature* **517**, 616–620

Received for publication August 12, 2018.
Accepted for publication January 22, 2019.

www.fasebj.org by Oxford Univ Lib Serv - Bodleian Lib (163.1.203.50) on June 11, 2019. The FASEB Journal Vol. ${article.issue.getVolume()}, No. ${article.issue.getIssueNumber()}